



Universiteit
Leiden
The Netherlands

The solid state photo-CIDNP effect

Daviso, E.

Citation

Daviso, E. (2008, November 18). *The solid state photo-CIDNP effect*. Retrieved from <https://hdl.handle.net/1887/13264>

Version: Corrected Publisher's Version

License: [Licence agreement concerning inclusion of doctoral thesis in the Institutional Repository of the University of Leiden](#)

Downloaded from: <https://hdl.handle.net/1887/13264>

Note: To cite this publication please use the final published version (if applicable).

PHOTO-CIDNP MAS NMR BEYOND THE T_1 LIMIT BY FAST CYCLES OF POLARIZATION EXTINCTION AND POLARIZATION GENERATION

2.1 INTRODUCTION

Magnetic resonance experiments are repeated to improve the signal-to-noise ratio by data accumulation. In the usual case, transitions of the detected nucleus or of a nucleus serving as a polarization source for cross-polarization are saturated as the result of the ($\pi/2$) pulse. The repetition frequency is then limited by the kinetics of equilibrium recovery of this nucleus (Figure 2.1A). This signal recovery depends on nuclear spin relaxation processes, which can be described phenomenologically by the three Bloch equations (Bloch, 1946). In particular, the longitudinal relaxation time T_1 characterizes the recovery of Boltzmann populations on a transition of a nuclear spin that interacts thermally with its surroundings. This kinetic parameter is a materials property and can be between milliseconds and several months (Levitt, 2001). For heavy nuclei such as ^{13}C in a rigid environment, as in the solid state, T_1 often is in the range of several seconds or minutes, providing a serious limit to the rate of signal accumulation. Recent developments of methods for polarization generation (PG) improve the sensitivity of NMR by several orders of magnitude by creation of transient highly polarized non-Boltzmann nuclear spin states, often termed as hyperpolarized states (Figure 2.1B). Examples for PG methods used in the solid state are optical pumping (Suter and Mlynec, 1991), dynamic nuclear polarization (DNP) (Becerra *et al.*, 1993), optical nuclear polarization (Stehlik, 1977), and the solid-state photo-CIDNP effect (Jeschke and Matysik, 2003; Daviso *et al.*, 2008a). In solids, photochemically induced dynamic nuclear polarization (photo-CIDNP) has been observed for the first time in quinone-blocked frozen samples of RCs of *Rb. sphaeroides* R26 under continuous illumination by MAS solid-state NMR (Zysmilich and McDermott, 1994). Until now, despite of plenty of efforts, the observation of the solid-state photo-CIDNP effect is limited to natural photosynthetic RCs (Roy *et al.*, 2008).

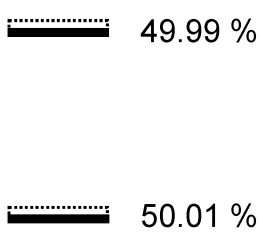
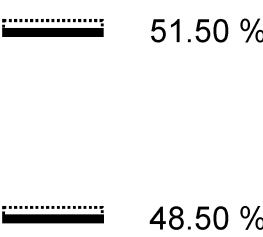
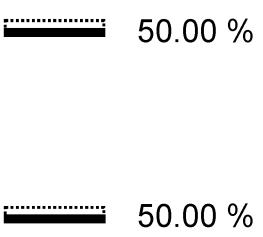
A	B	C
β  49.99 % 50.01 % α	β  51.50 % 48.50 % α	β  50.00 % 50.00 % α
Boltzmann distribution	Hyperpolarized states	Polarization extinction

Figure 2.1: Different regimes of population of the nuclear spin two-level system. (A) Boltzmann distribution for an ensemble of spins at thermal equilibrium. (B) Emissive hyperpolarization induced by the solid-state photo-CIDNP effect. The typical values of nuclear spin population in a NMR experiments are in between state A and B. (C) Saturation of the transition after polarization extinction (PE).

Using continuous illumination, photo-CIDNP has been observed by MAS NMR in purple non-sulphur bacterial RCs from *Rb. sphaeroides* WT and R26 (Prakash *et al.*, 2005a; 2006), RCs from the green sulphur bacterium *Chlorobium tepidum* (Roy *et al.*, 2007), of the heliobacterium *Heliobacillus mobilis* (Roy *et al.*, 2008) as well as in plant photosystems I and II (Matysik *et al.*, 2000a; Alia *et al.*, 2004; Diller *et al.*, 2005; Diller *et al.*, 2007a). In addition, NMR signals were detected in entire membrane-bound photosynthetic units (Prakash *et al.*, 2003) and whole cells of *Rb. sphaeroides* (Prakash *et al.*, 2006). Photo-CIDNP MAS NMR intensities are related to the local electron spin densities in the electron donor and the electron acceptor in the radical pair state. The origin of the solid-state photo-CIDNP effect in photosynthetic RCs has been explained by the parallel occurrence of up to three mechanisms (Jeschke and Matysik, 2003; Prakash *et al.*, 2005a; 2006; Daviso *et al.*, 2008a). The TSM (Jeschke, 1997; 1998) depends on the coupling between two electron spins in a radical pair state, leading to enhanced nuclear polarization of the cofactors involved, which is transferred by anisotropic hf coupling into coherent evolution of electron spins. The DD mechanism (Polenova and McDermott, 1999) does not require electron-electron coupling if spin-correlated radical pairs have different lifetimes in their S and T_0 states. In both mechanisms, high nuclear polarization is built up within hundreds of nanoseconds till microseconds by hfi of the correlated electron radical pair with nuclei. The third mechanism is active in systems having a long-living T

state, which eventually leads to the DR between the nuclear spins in the triplet and in the ground state of P (Goldstein and Boxer, 1987; McDermott *et al.*, 1998). In WT RCs, the DR mechanism does not occur since nuclear spin longitudinal relaxation is negligible during the triplet lifetime of the donor of 100 ns, while in R26 RCs a donor triplet lifetime of 100 μ s is sufficiently long to observe this effect. In photo-CIDNP MAS NMR, nuclear PG opens up additional polarization loss channels and therefore leads to enhanced signal recovery compared to longitudinal relaxation in the absence of PG (Diller *et al.*, 2007b).

Combination of the photo-CIDNP effect with selective isotope labelling allows for further increase of sensitivity and selectivity. Upon isotope labelling, natural spin diffusion spreads the nuclear polarization into the vicinity of the active cofactors. The effect is used in continuous illumination experiments to map the electronic ground-state of the entire active cofactors as well as their surrounding amino acids of the protein (Matysik *et al.*, 2001a; 2001b; Schulten *et al.*, 2002; Prakash *et al.*, 2007). On the other hand, spin diffusion leads to a redistribution of the primary polarization and obscures the primary photo-CIDNP MAS NMR intensities which provide information on electron spin densities. While such spin diffusion in photo-CIDNP MAS NMR experiments on selectively isotope labelled samples allows to obtain chemical shift information of an area beyond the radical pair, it thus makes a reconstruction of the electron spin density distributions difficult. In contrast, laser-flash photo-CIDNP MAS NMR experiments allow both to obtain the true electron spin densities and to observe the ground-state information of the radical pair as well as its surroundings. Furthermore, the application of laser flashes enables time-resolved photo-CIDNP MAS NMR experiments. Hence, laser-flash photo-CIDNP MAS NMR experiments allow for studying the mechanism that generates photo-CIDNP in great detail, while continuous illumination experiments show only a net effect and average information on the electronic structure of the radical pair state. In order to perform such time-resolved experiments with a well defined initial state of the spin system and with a maximum possible repetition rate, any coherence and polarization still existing before the start of a new experiment needs to be extinguished. Otherwise residual polarization builds up during subsequent photo-cycles, as recently discussed in detail (Diller *et al.*, 2007b) and may be transferred by spin diffusion to nuclei that are not polarized in the primary event.

The present chapter is concerned with the technique of polarization extinction (PE) by equalizing the populations at the two levels of a nuclear spin transition before PG event (Figure 2.1C). As a consequence of such presaturation, the memory of the spin system is

erased and the experiment detects only processes initiated by the next PG event. In the literature, a few cases of optimized PE, exclusively of ^1H liquid-state NMR, have been reported (Schäublin *et al.*, 1977; Closs and Miller, 1979; Mok and Hore, 2004; Kuprov *et al.*, 2005; Goetz *et al.*, 2006), for example using WALTZ-16 for fast time-resolved liquid-state ^1H photo-CIDNP studies (Morozova *et al.*, 2004). Early DNP experiments on solids worked with add-subtract pulse sequences to eliminate effects of residual polarization (Afeworki *et al.*, 1992). Presaturation of ^1H transitions by a train of an unspecified number of $(\pi/2)$ pulses was employed in recent work on DNP generated by biradicals (Hu *et al.*, 2004).

Here we present for the first time time-resolved laser-flash photo-CIDNP MAS NMR data, which have been obtained by application of the proposed PE-PG strategy. This strategy combines optimized polarization extinction (PE) with polarization generation (PG) to allow for accumulation of time-resolved NMR data with repetition times much shorter than T_1 . The new time limit on the repetition rate in such PE-PG experiments is given either by the minimum recycle delay of the NMR spectrometer or by the maximum repetition rate of the laser. The significant speed-up of accumulation allows for more sensitive measurements on short-lived chemical states.

2.2 MATERIALS AND METHODS

2.2.1 Sample preparation

Cultures of *Rb. sphaeroides* WT (480 mL) were grown anaerobically in the presence of 1.0 mM [4- ^{13}C]- δ -aminolevulinic acid-HCl (ALA), which was purchased from Cambridge Isotope Laboratories (99% ^{13}C -enriched). The cultures were allowed to grow for 7 days in light. The culture was centrifuged for 10 minutes at $5500 \times g$ and the combined pellet was resuspended in 40 mL 0.1 M phosphate buffer. The RCs were isolated as described by Shochat *et al.* (1994). A protein/pigment ratio $A_{280}/A_{802} = 1.2$ was measured in the absorption spectrum to assess the purity of the samples. Approximately 15 mg of the labeled RC protein was used for the NMR experiments. The measurement of ^{13}C -isotope content has been achieved as described by Schulten *et al.* (2002).

2.2.2 MAS NMR measurements

The NMR experiments were performed on a Avance DRX-200 NMR (Bruker-Biospin GmbH, Karlsruhe, Germany). All NMR spectra of histidine have been obtained at a temperature of 298 K and at a spinning frequency of 8 kHz. The spectra were collected using a spin echo pulse sequence with the CYCLOPS phase cycle of the ($\pi/2$) pulse under TPPM carbon-proton decoupling (Bennett *et al.*, 1995). A total number of 512 scans per spectrum have been collected.

Photo-CIDNP spectra were obtained at a temperature of 243 K and at a spinning frequency of 8 kHz. The photo-CIDNP MAS NMR spectra were collected using a spin echo pulse with the CYCLOPS phase cycle of the ($\pi/2$) pulse under TPPM carbon-proton decoupling. A total number of 67k scans per spectrum was collected. The optimum length of the ($\pi/2$) carbon pulse, determined on uniformly ^{13}C labeled histidine, varies from 4.8 to 5.0 μs under our experimental conditions using a rf power of ~ 250 W. The phases of the pulses in PE-PG pulse sequences as shown in Figures 2.2 and 2.6 are:

$$\phi_1 = +x -x +x -x +x -x +x -x +x -x +x -x +x -x +x -x$$

$$\phi_2 = +x +x +y +y -x -x -y -y +x +x +y +y -x -x -y -y$$

$$\phi_3 = +y +y -x -x +y +y -x -x -y -y +x +x -y -y +x +x$$

$$\phi_4 = +x +x +y +y -x -x -y -y +x +x +y +y -x -x -y -y$$

2.3 EXPERIMENTAL

The set up for fast PE-PG experiments combines a nanosecond-flash laser set-up with a modified MAS NMR spectrometer (Figure 1.12).

2.3.1 Nanosecond-flash laser set-up

A pulsed nanosecond (ns)-flash laser provides sufficient radiation intensity for time resolved photo-CIDNP MAS NMR studies and does not decrease the time-resolution which can be obtained in NMR experiments. The laser is operating with a repetition rate between 1 and 10 Hz. Using 1064-nm flashes of a Nd:YAG laser (SpectraPhysics Quanta-Ray INDI 40-10, Irvine CA, USA), upon frequency-doubling with a second harmonic generator (SHG), 532-nm laser flashes with pulse length of 6-8 ns and an energy between 20 to 270 mJ at 1-4 Hz are produced.

2.3.2 Electronic coupling of laser and NMR

The NMR console is used as master, while the laser is running in the mode of a slave. The connection is provided by a DDG (Model 9650A, PerkinElmer, Waltham, USA). The spectrometer generates the triggering impulse via a TTL channel for the DDG. The DDG triggers both pump lamp and Q-switch with a delay between 150 and 230 μs in order to have optimum control of the energy output. The synchronization of the laser light pulse with the NMR rf pulse can be verified with a 500-MHz oscilloscope (Series TDS3000B, Tektronix, Beaverton, USA) connected to the output channel of the spectrometer as well as to a photodetector. The photodetector consists of a fast photodiode (FND-100, EG&G, Salem, USA) and a custom-made amplifier. The timing precision of the combined optical and NMR experiment has been demonstrated to be about ± 1 ns (Davis *et al.*, 2008a). Note, however, that the time resolution of photo-CIDNP experiments is limited by the length of the $(\pi/2)$ ^{13}C rf pulse used for NMR excitation. A typical value of this parameter is 5 μs .

2.3.3 Optical coupling of laser and NMR

Radiation emitted by the laser is transferred to the sample via a fiber bundle (FiberTech GmbH, Berlin, Germany). A multi-mode light fiber bundle provides high optical transparency in a broad spectral range as well as sufficient mechanical flexibility for being attached to the stator of the MAS probe. The optically active diameter is 3 mm and the numerical aperture is 0.22. The ratio of the radiation energies between input and output powers of the fiber bundle is 0.25. A Galilean lens system and a multi-mode fiber aligner are used for coupling the radiation pulses into the fiber bundle. The Galilean lens system, combining a concave lens with a convex one, allows collimation of the beam to the diameter required.

The MAS NMR probe head (Avance DRX-200, Bruker-Biospin GmbH, Karlsruhe, Germany) has been modified in order to illuminate the rotor from the side (Matysik *et al.*, 2000b). This includes (a) a bore drilled into the most upper partition plate separating stator chamber and electronics, (b) drilling a small opening into the stator, and (c) winding a new coil from thin silver wire. The samples have been loaded into optically transparent sapphire MAS rotors to ensure homogeneous illumination.

2.4 THEORY

2.4.1 General considerations

High time-resolution can be obtained by excitation of the electronic states with a ns laser flash. However, such experiments lack the advantage of a build-up of polarization during repeated photo-cycles that is inherent in experiments with continuous illumination. Such build-up leads to further signal enhancement by a factor between 5 and 90, depending on the system under consideration (Diller *et al.*, 2007b). This sensitivity loss of a time-resolved compared to a continuous experiment can at least partially be compensated by faster repetition, as the signal recovery in continuous illumination experiments is linked to T_1 in the seconds to minutes range, while the signal in time-resolved experiments is generated on timescales between tens of nanoseconds and hundreds of microseconds. In practice, another limit may be imposed by the maximum technically feasible repetition rate of the laser and NMR pulses. However, this is still significantly faster than thermal equilibration of the spin system, in particular, since equilibration may also involve slow processes of polarization exchange with remote nuclei via spin diffusion.

A time-resolved experiment consists of PG by laser excitation, a variable evolution period, and NMR detection. After these steps, the nuclear spin system is generally in a not very well defined non-equilibrium state. To start the next repetition of the experiment in a well-defined state, any remaining coherence and polarization have to be extinguished. Coherence decays with the transverse relaxation time T_2 , which in solids is on the time scale of milliseconds. As the detection period of an NMR experiment usually lasts until coherence has completely decayed and as the limit imposed by T_2 on the permissible repetition rate is less stringent than the limits imposed by the maximum allowed duty-cycle of the NMR spectrometer and maximum repetition rate of the laser, coherence is of no particular concern here. If coherence needs to be extinguished, the probehead should be fitted with a coil for supplying a PFG along z . The phase of any coherence remaining after the experiment can then be scrambled by a single field gradient pulse (Maas *et al.*, 1999).

However, as T_1 in solids usually exceeds technical limits on the repetition time, residual nuclear polarization needs to be extinguished. For optimum performance, PE should be as complete as possible and should be achieved with a minimum number of pulses in a time that is sufficiently short to not impose another limit on the repetition rate. Minimization of the number of pulses is required to avoid excessive rf heating during fast

repetition. Although in our current implementation, rf heating results almost exclusively from proton decoupling, use of new techniques for weak-power decoupling at high MAS speed (Ernst *et al.*, 2004) would enhance the importance of power insertion by the presaturation sequence.

The presaturation sequence needs to be as short as possible, since polarization recovery by longitudinal relaxation and back transfer from remote nuclei, polarized via spin diffusion, compete with PE. Furthermore, sequence design has to consider imperfections in experimental setup as well as rf inhomogeneity, *i.e.*, it should perform reasonably well for slight maladjustments of the flip angles of the presaturation pulses. Any phase cycling introduced in the presaturation sequence to suppress residual polarization must result in a constant detection phase. This is because the phase of the actual signal does not depend on settings in the presaturation sequence. In the following, we consider sequences of $(\pi/2)$ pulses with such additive phase cycling and discuss how the other conditions can be met.

2.4.2 Residual polarization

After a single $(\pi/2)$ pulse, some polarization remains as the flip angle has a small error δ . This error may slightly vary with resonance offset λ as well as across the sample due to inhomogeneity of the rf field. If the polarization before the pulse is described by the effective density operator

$$\tilde{\sigma}_0 = p I_z, \quad (2.1)$$

where I_z is the z -component of the spin angular momentum and p is the initial polarization. The resulting effective density operator after a pulse with phase $+x$ is given by

$$\tilde{\sigma}_1 = -p \cos \delta I_y + p \sin \delta I_z. \quad (2.2)$$

Polarization does not evolve during the periods of free evolution. Hence, neglecting for the moment any conversion of coherence back to polarization by later pulses, the residual polarization after n nominal $(\pi/2)$ pulses is

$$p_1 = p \sin^n \delta. \quad (2.3)$$

Equation (2.3) is valid for all signals, independently of their chemical shift or resonance offset λ , except for a possible minor variation of δ with resonance offset. The required number n of pulses thus depends on the quality of PE needed and on the mean flip angle error $\langle \delta \rangle$. The contribution to the residual polarization described by Equation

(2.3) cannot be cancelled by phase cycling, as it does not depend on the phase of the first ($\pi/2$) pulse and only additive phase cycles are permissible. In contrast, the coherence created by the first pulse can be extinguished by additive phase cycling. The effective density operator after a first pulse with phase $-x$ is given by

$$\tilde{\sigma}_1' = p \cos \delta I_y + p \sin \delta I_z, \quad (2.4)$$

so that a $[(+x)+(-x)]$ cycle on this pulse leaves only the residual polarization term. Due to a small deviation $\Delta\phi$ in the relative phases of the $+x$ and $-x$ pulses from 180° , a minor fraction $p_2 = [2(1-\cos \Delta\phi)]^{1/2} p \ll p$ of the coherence may survive such phase cycling. Alternatively, if a PFG setup is available, the coherence can be destroyed by a field gradient pulse.

A second pulse will reconvert part of the coherence (transverse magnetization) to polarization. To quantify this, we have to consider evolution and relaxation of the coherence during interpulse delay t_{ip} between the $\pi/2$ pulses that we associate with time d_2 in Figure 2.2. Before the second pulse we find

$$\begin{aligned} \tilde{\sigma}_2 = & -p_2 \exp(-t_{ip}/T_2) \cos \delta \cos(\lambda t_{ip}) I_y \\ & + p_2 \exp(-t_{ip}/T_2) \cos \delta \sin(\lambda t_{ip}) I_x + p \sin \delta I_z. \end{aligned} \quad (2.5)$$

After this pulse the density operator is described by

$$\begin{aligned} \tilde{\sigma}_3 = & -p_2 \exp(-t_{ip}/T_2) \cos^2 \delta \sin(\lambda t_{ip}) I_z \\ & + p_2 \exp(-t_{ip}/T_2) \cos \delta \sin(\lambda t_{ip}) I_x - p \sin \delta \cos \delta I_y + p \sin^2 \delta I_z. \end{aligned} \quad (2.6)$$

Note that the last term on the right-hand side of Equation (2.6) corresponds to the contribution described by Equation (2.3) with $n=2$. In Equation (2.6), $\sin(\lambda t_{ip})$ can have any value in the range between -1 and 1 . Thus, the contribution to residual polarization from reconversion of coherence is given by

$$|p_3| \leq p_2 \exp(-t_{ip}/T_2) \cos^2 \delta, \quad (2.7)$$

with the actual magnitude depending on the resonance offset λ . This contribution can be minimized by prolonging t_{ip} . On the other hand, prolonging t_{ip} leads to some signal recovery by longitudinal relaxation. Assuming that p is an equilibrium polarization this creates an additional contribution

$$p_4 = p \left[1 - \exp(-t_{ip}/T_R) \right], \quad (2.8)$$

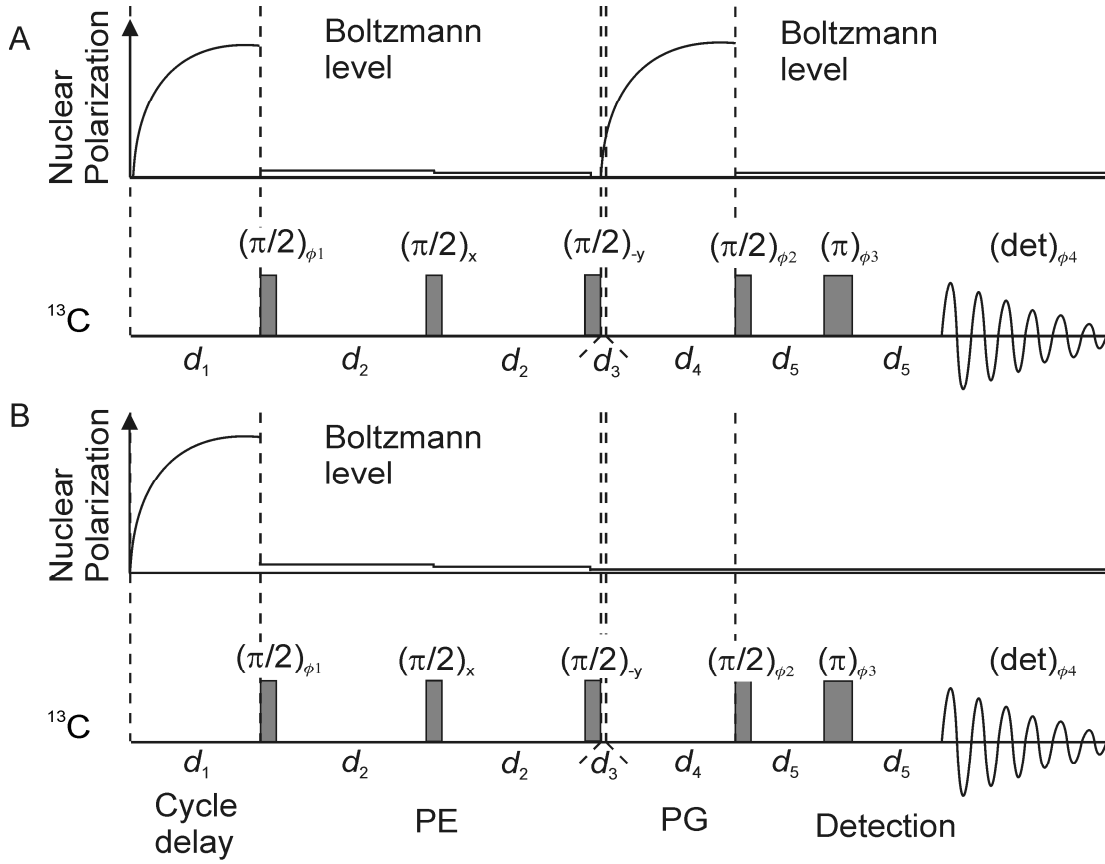


Figure 2.2: Pulse sequence for a PE-PG experiment with longitudinal relaxation serving as PG step. (A) $d_1 = 12$ s, $d_2 = 20$ ms, $d_3 = 1$ ms, $d_4 = 12$ s, $d_5 = 125$ μs (1/8000 Hz, *i.e.*, one period of the MAS frequency), $d_{\text{detection}} = 40$ ms. (B) as before, but with $d_4 = 200$ μs .

where the recovery time T_R equals T_1 in the absence of illumination but can be shorter during continuous illumination for those signals that exhibit a photo-CIDNP effect (Diller *et al.*, 2007b). To optimize the sequence, t_{ip} needs to be adjusted so that the sum of p_3 and p_4 is minimized. Usually one has $T_R \gg T_2$ in solids. If $t_{\text{ip}} \gg T_2$ and $t_{\text{ip}} \ll T_R$ can be fulfilled simultaneously, both p_3 and p_4 are negligible with respect to p_1 . In this situation the total residual polarization is well approximated by Equation (2.3) for any number n of pulses. This is the situation that we meet in the experimental examples in this work. If T_R and T_2 are too close to each other to fulfil both these conditions, additional additive phase cycling has to be introduced. A phase cycle $[(+x, +x) + (-x, +x) + (+x, -x) + (-x, -x)]$ applied to the two presaturation pulses eliminates contribution p_3 except for a residual term p_5 of the order $2(1 - \cos \Delta\phi) \exp(-t_{\text{ip}}/T_2) p$. The polarization after a two-pulse presaturation sequence is then given by

$$p_6 = p \sin^2 \delta + p_5. \quad (2.9)$$

Note that p_5 is a signed quantity that depends on the resonance offset λ . For sequences with n pulses, complete additive phase cycling of all pulses (2^n steps) or field

gradient pulses of sufficient amplitude and duration after each $(\pi/2)$ pulse should be applied.

2.4.3 Relative phase of the pulses

Consider the pulse sequence $(\pi/2)_{\phi_1-t_{ip}}-(\pi/2)_{\phi_2}$. In a well resolved spectrum, the variance σ_λ of the resonance offset λ is much larger than the linewidth $1/T_2$. If $t_{ip} > T_2$, we thus have $\lambda t_{ip} \gg 2\pi$ for typical λ values. Hence, after time t_{ip} has passed, the phase of the coherence for different nuclei is distributed over the whole possible range $(0, 2\pi)$. In a magnetization vector picture, transverse magnetization for the different nuclei is distributed over the whole xy plane. In this situation the relative phase of two consecutive pulses cannot be optimized for signal suppression throughout the whole spectrum.

If coherence reconversion is suppressed by complete additive phase cycling rather than by relaxation, $t_{ip} \ll T_2$ and hence $t_{ip} \ll 1/\sigma_\lambda$ can be chosen. In this situation coherence reconversion by the second pulse in a pair of $\pi/2$ pulses is further diminished if this pulse has a phase shift of $\pm 90^\circ$ with respect to the first pulse. We implement this phase shift for the last two pulses in our presaturation sequence. Note that the 90° phase shift is compatible with additive phase cycling. The complete presaturation sequence is thus given by

$$(\pi/2)_{\phi_1-t_{ip}} - \left[(\pi/2)_{\phi_i-t_{ip}} \right]_{n-2} - (\pi/2)_{\phi_n} - T, \quad (2.10)$$

where time T between the last pulse of the presaturation sequence and the polarization generation should be kept as short as possible to prevent unnecessary polarization recovery.

In this we assume that the polarization generator does not reconvert the small residual nuclear coherence to polarization. Phase ϕ_1 is generally cycled $+x/-x$ with addition of both signals. For $T_R \gg T_2$, we use $T_2 < 3 t_{ip} \ll T_R$ and constant phases $\phi_i = +x$ and $\phi_n = -y$.

For $T_R \approx T_2$, each of the pulses in the square brackets in Eq. (2.10) should be phase cycled individually with $\phi_i = +x/-x$ with addition of the signals and the last pulse should be cycled with $\phi_n = -y/+y$ with addition of the signals. In this regime an odd number n of pulses gives better results than an even number, as the final reconversion of coherence to polarization is avoided. Unless $t_{ip} \gg T_2$ can be chosen, an odd number of pulses is also advantageous in the regime $T_R \gg T_2$. The phase cycle of the presaturation sequence is combined with usual CYCLOPS phase cycling for the detection sequence.

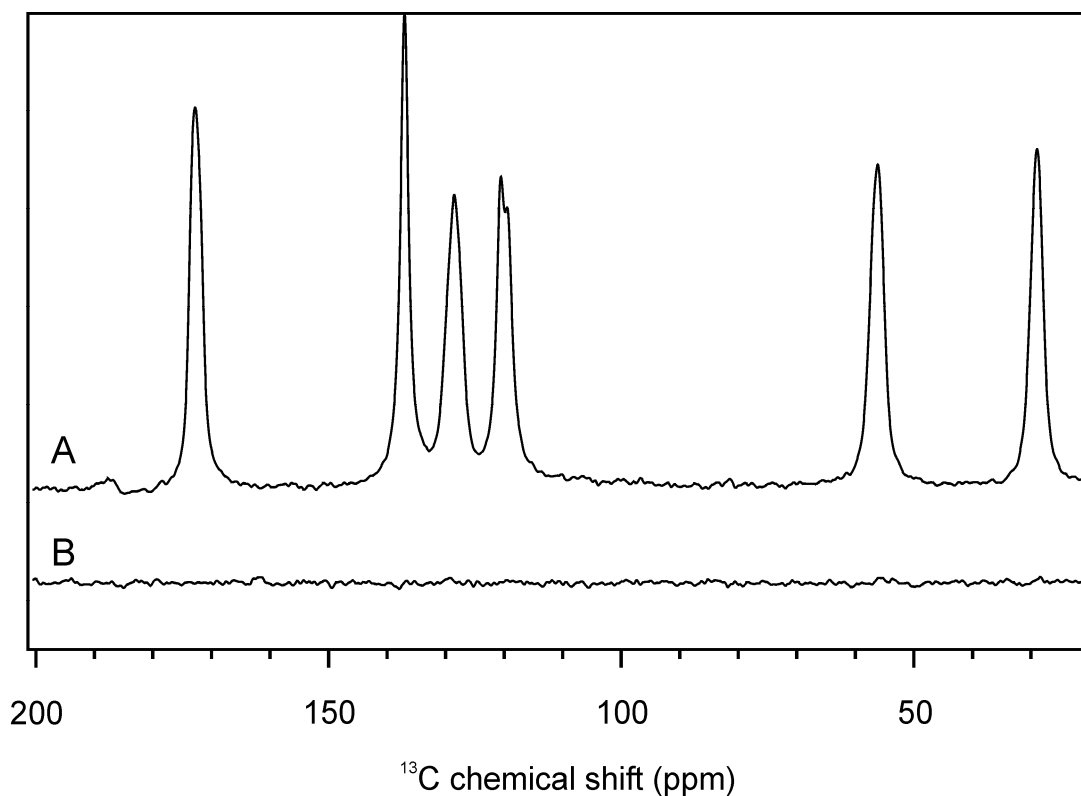


Figure 2.3: Efficiency of polarization extinction (PE) for solid histidine. (A) Spectrum obtained according to Trace A in Figure 2.2 with a delay $d_1 = d_4 = 12$ sec. (B) Spectrum obtained according to Trace B in Figure 2.2 with a delay $d_1 = 12$ sec and $d_4 = 200$ μ s.

2.5 RESULTS AND DISCUSSION

2.5.1 PE-PG experiments on histidine

The PE-PG pulse sequences are constructed of four building blocks: recycle delay, PE, PG and detection (Figures 2.2 and 2.6). In both sequences, PE is caused by a train of $n = 3$ pulses with flip angle $\pi/2$ of which only the first one is phase cycled $[(+x)+(-x)]$.

Experimentally, we found useful minimum values of about 200 ms corresponding to twice the limit imposed by the laser. In addition to phase cycling, we use an interpulse delay d_2 of 20 ms, which is significantly longer than T_2 , so that conversion of coherence to polarization can be neglected.

In the case of histidine, PG is simply a relaxation delay d_4 during which polarization recovery towards thermal equilibrium occurs. The two extreme cases for a Boltzmann spin system are shown in Figure 2.2. Long delays allow for complete signal recovery (Trace A in Figure 2.2), while for short delays the build-up of Boltzmann polarization is negligible (Trace B in Figure 2.2). Hence, experiments on histidine can be used for probing the efficiency of presaturation. Figure 2.3 shows two spectra of uniformly ^{13}C -labeled histidine. Both spectra have been measured using a spin echo pulse sequence

with a recycle delay d_1 of 12 s. Trace A in Figure 2.3 shows the presaturation pulse sequence that has been used by imposing the relaxation delays d_1 and d_4 to 12 s, according to the polarization evolution shown by Trace A in Figure 2.2.

An experiment as shown by Trace B in Figure 2.2 leads to Trace B in Figure 2.3, which has been collected with a short relaxation delay d_4 of 200 μ s, corresponding to a total recovery time d_3+d_4 of 1.2 ms. Under these conditions, the signal is almost extinguished. Considering the magnitude spectra of both experiments, the ratio between the integrals of all signals B/A is <0.25 %. For a longitudinal relaxation time of 10 s and a recovery time of 1.2 ms, only 0.012% of signal recovery would be expected. This indicates that the small residual signals are due to incomplete PE. However, a suppression of more than 99.75% of the initial polarization is certainly sufficient for solid-state NMR experiments with hyperpolarization, in which data are rarely accumulated to signal-to-noise ratios larger than 400.

The effect of the number of ($\pi/2$) PE pulses has been investigated. Using three ($\pi/2$) PE pulses leads to the best results (Trace C in Figure 2.4). With $n = 1$ and 2, significantly larger residual signals were observed (Traces A and B in Figure 2.4), while $n = 4$ (Trace D in Figure 2.4) did not lead to significant improvements with respect to $n = 3$. Using three ($\pi/2$) PE pulses, the influence of d_2 on PE is explored in Figure 2.5.

Short d_2 values lead to imperfect PE (Traces A and B in Figure 2.5), while a d_2 of 20 ms, *i.e.* T_2 value of Histidine at our experimental conditions, is sufficiently long to allow for almost complete PE (Trace C in Figure 2.5). The data clearly demonstrate that d_2 values longer than T_2 are required to erase the signal, if only the first ($\pi/2$) pulse is phase cycled.

The residual signals observed with $n = 1$ or 2 presaturation pulses are clearly out of phase, suggesting that they do not originate from a spin echo coherence transfer pathway. A complete 32-step phase cycle that combines $[+(+y)-(-x)+(-y)-(+x)]$ cycling on the (π) pulse with CYCLOPS on the ($\pi/2$) pulse of the echo subsequence and the additive phase cycling should cancel these signals and lead to improved performance.

2.5.2 Time-resolved ^{13}C PE-PG photo-CIDNP MAS NMR

In photo-CIDNP MAS NMR, PG occurs during a photo-cycle which is completed after a time of a few hundred nanoseconds to a few hundreds of microseconds, depending on the sample under consideration.

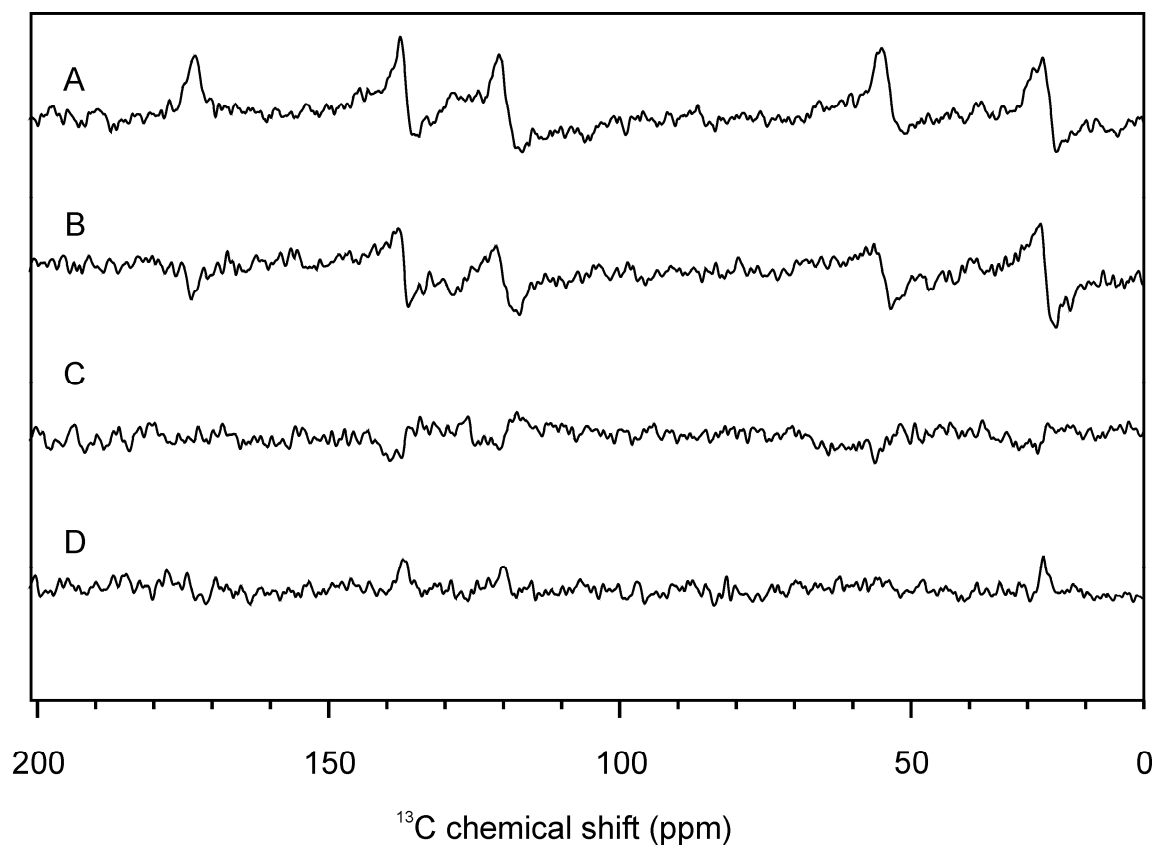


Figure 2.4: Comparison of the efficiency of presaturation pulse sequences having (A) one, (B) two, (C) three and (D) four ($\pi/2$) pulses for solid histidine. For the presaturation pulse sequences with more than one ($\pi/2$) pulse, the delay time d_2 is 20 ms.

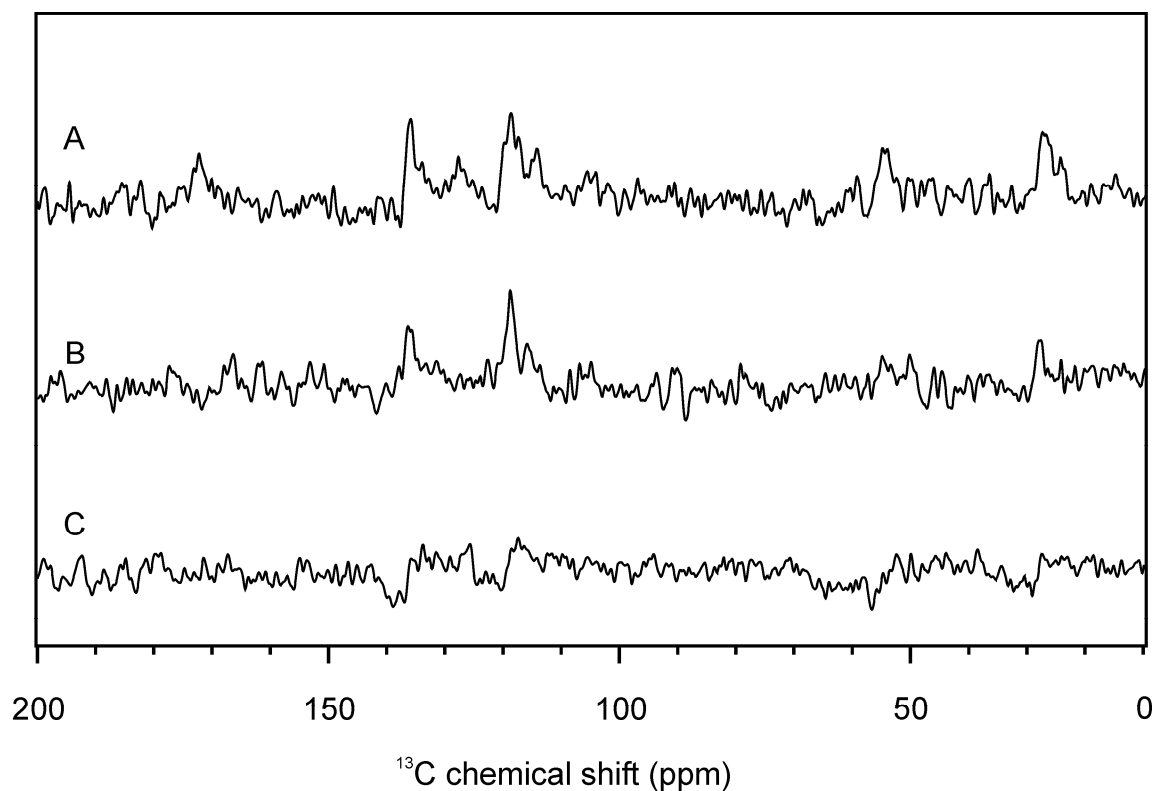


Figure 2.5: Comparison of the efficiency of presaturation pulse sequences having three ($\pi/2$) pulses with different delay times d_2 of (A) 5 ms, (B) 10 ms and (C) 20 ms. The sample is solid histidine.

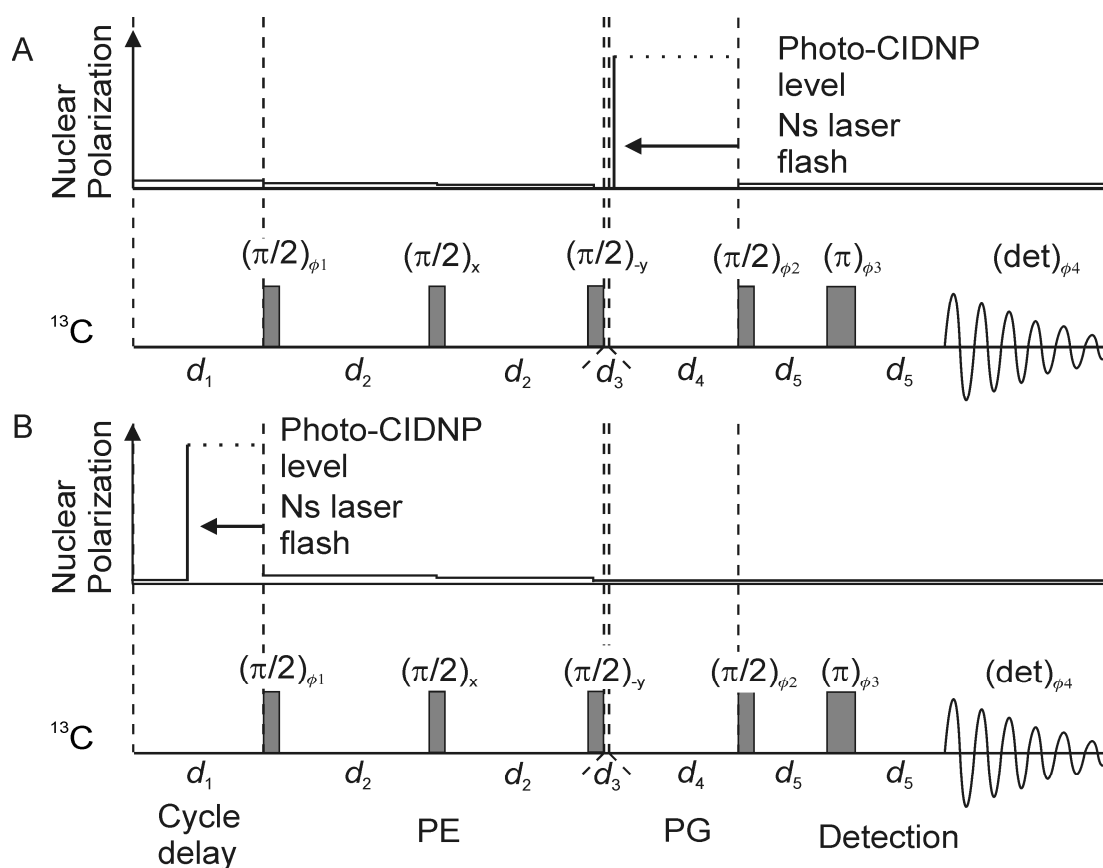


Figure 2.6: Pulse sequence for a PE-PG experiment based on ns-laser flash photo-CIDNP MAS NMR. (A) Laser flash during the polarization generation (PG) period. Values used for obtaining Trace A in Figure 2.7 are: $d_1 = 200$ ms, $d_2 = 20$ ms, $d_3 = 1$ ms, $d_5 = 125$ μs ($1/8000$ Hz, *i.e.*, one period of the MAS frequency), $d_{\text{detection}} = 30$ ms, d_4 is 2 ms (A), 60 ms (B), 133 ms (C) and 500 ms (D). (B) Laser flash, *i.e.* PG, before the polarization extinction (PE) period. Values used to obtain Trace F in Figure 2.7 are as before, but $d_4 = 500$ ms.

Using a nanosecond-laser flash, d_4 is not considered as relaxation delay but as the time delay between optical excitation and NMR detection (Trace A in Figure 2.6). For capturing the earliest events, d_4 should be as short as the hardware allows. A strong solid-state photo-CIDNP effect has been observed with 4-ALA labeled WT RCs under continuous illumination under white light (Matysik *et al.*, 2001b; Schulten *et al.*, 2002) leading to entirely negative signals (Prakash *et al.*, 2005a). Figure 2.7 shows a series of four spectra (traces A to D) of this sample obtained with different delay times between laser pulse and NMR detection. Already at a d_4 delay of 2 ms (Trace A in Figure 2.7), strong signals appear exclusively in the aromatic region of the ^{13}C NMR spectrum. This is in contrast to previous experiments under continuous illumination, in which also light-induced signals appear in the aliphatic region (Matysik *et al.*, 2001b; Schulten *et al.*, 2002).

Data obtained at 60, 133 and 500 ms (Traces B, C and D in Figure 2.7) show the exact kinetics of polarization transfer to the aliphatic carbons on the ms timescale which

can be understood in terms of spin diffusion towards the steady-state envelope (Trace E in Figure 2.7).

The differences between the laser-flash experiment with a long delay d_4 (Trace D in Figure 2.7) and the steady state spectrum (Trace E in Figure 2.7) is due to relaxation and further spin diffusion occurring under steady state conditions. The positive signals observed at the longer times can be assigned to the protein. They are not due to a solid-state photo-CIDNP effect but rather due to recovery of thermal polarization by the 3300 methyl carbons of the protein backbone caused by the increased d_4 delay. As a matter of fact, these resonances appear also in the dark spectrum collected using a PG period of 500 ms (Trace F, Figure 2.7). These data demonstrate that with PE-PG strategy nuclear polarization buildup and transfer can be observed with a time resolution in the millisecond range. For proving the efficiency of PE in the photo-CIDNP MAS NMR experiment, the laser pulse is shifted before the presaturation into the d_1 cycle delay (Trace B in Figure 2.6). Under these conditions, no significant solid-state photo-CIDNP effect appears (Trace F in Figure 2.7).

2.6 CONCLUSIONS

In traditional NMR, polarization is too valuable to consider PE. Modern methods for fast and efficient PG, such as those using the solid-state photo-CIDNP effect, however, have a signal build-up independent of T_1 and require fast-cycling PE-PG experiments for obtaining optimum sensitivity enhancement. PE is also required for time-resolved observation of polarization build-up in such experiments, as interference by polarization from previous photo-cycles has to be avoided. We have shown that the repetition rate can be dramatically reduced from 1 scan per 17 seconds, as required for optimum recovery of thermal equilibrium polarization, to about 4 scans per second. The new limit is imposed by restrictions of the NMR hardware. We have further demonstrated that under these conditions, kinetic experiments with millisecond time-resolution are virtually undisturbed by residual polarization from previous photo-cycles. It appears reasonable to expect that polarization build-up and transfer can also be observed on the microsecond time-scale. A similar PE-PG strategy may also be applicable to MRI, for instance in conjunction with the use of hyperpolarized gases in lung imaging or dissolved in the bloodstream, to safely assign observed contrast to a certain time after injection of the hyperpolarized contrast agent (Daviso *et al.*, 2008b).

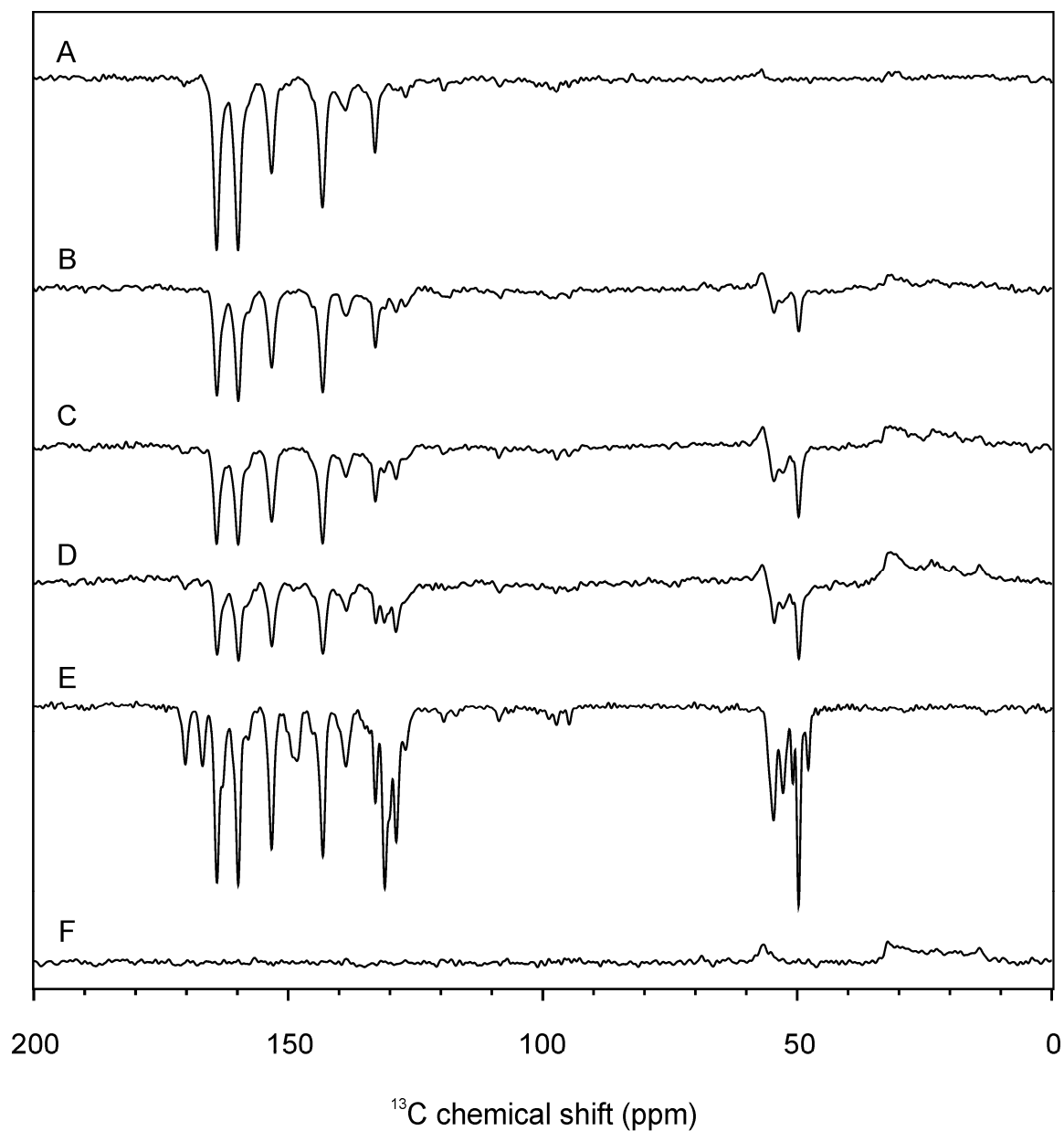


Figure 2.7: Nanosecond-laser flash photo-CIDNP MAS NMR on *Rb. sphaeroides* wild type photosynthetic reaction centers obtained with the sequence according to Trace A in Figure 2.6 and four different values of d_4 being (A) 2 ms, (B) 60 ms, (C) 133 ms and (D) 500 ms. (E) Continuous illumination photo-CIDNP MAS NMR spectrum of *Rb. sphaeroides* wild type photosynthetic reaction center. (F) Spectrum obtained with the sequence according to Trace B in Figure 2.6.

